Distributed Control of Networked Microgrid with Heterogeneous Energy Storage Units Considering Multiple Types of Time Delays

Guoxiu Jing, Bonan Huang, Rui Wang, Chao Yang, and Qiuye Sun, *Senior Member*, *IEEE*

***Abstract*—This paper focuses on the distributed control problem in a networked microgrid (NMG) with heterogeneous energy storage units (HESUs) in the environment considering multiple types of time delays, which include the state, input, and communication delays. To address this problem, a state feedback control (SFC) strategy based on nested predictor is proposed to mitigate the influence of multiple types of time delays. First, a distributed control method founded upon voltage observer is developed, which can realize proportional power distribution according to the state of charge (SOC) of the HESUs, while adjusting the average voltage of the point of common coupling (PCC) bus in the NMG to its rated value. Then, considering that there exists steady-state error resulting from the initial value of the observer and impact of time delays, an SFC strategy is proposed to further improve the robustness of the NMG against time delays. Finally, the experimental results demonstrate that the proposed distributed control method is capable of fully compensating for the state, input, and communication delay. Moreover, the NMG exhibits remarkable resistance to multiple types of time delays, which has higher reliability and robustness.**

***Index Terms*—Networked microgrid (NMG), heterogeneous energy storage unit (HESU), distributed control, time delay.**

I. Introduction

THE goal of achieving net-zero energy requires an increasing proportion of net-zero distributed energy resources (DERs). Microgrid (MG) can integrate net-zero DERs, such as wind power, solar power, and other alternative energy sources without carbon emissions to achieve this goal. Considering the limited power generation capacity and specific geographic boundaries of a single MG, the most commonly used method is to interconnect multiple MGs to construct a networked microgrid (NMG). In addition, the NMG demonstrates robust resilience against extreme events. Therefore, in order to further enhance the reliability and resilience of the power system, traditional MGs are transformed into a larger and more complex NMG [1]-[3]. However, the intermittency, randomness, and power fluctuation of DERs threaten the reliable operation of the NMG, which pose new challenges to the cooperative control of the NMG [4], [5].

Energy storage systems (ESSs) are indispensable for the efficient utilization of DERs, as they enable flexible energy conversion and eliminate the need for simultaneous power generation, transmission, and distribution. This plays a significant role in enhancing the efficiency of the power system [6]-[8]. Therefore, it is necessary to configure multiple sets of distributed heterogeneous energy storage units (HESUs) to address the uncertainty of net-zero DERs in the NMG system. Moreover, due to different usage requirements, HESU exhibits dynamics, uncertainties, as well as functional, parameteric, and informative asymmetry [9], [10]. These characteristics pose challenges for distributed control. Recently, the existing studies primarily focused on studying the theory of distributed control [11]-[17]. For example, the distributed control strategy in [13] is designed to realize voltage regulation and power sharing within the MG. Meanwhile, an event-triggered communication mechanism is employed to ensure accurate current sharing and achieve desirable performance in the MG [12]. However, the above-mentioned studies are all designed for a single MG. In contrast, the NMG with net-zero DERs has a complex topology and operational characteristics, which require the development of an adaptable and robust control approach to addressing these variations and ensure the stability of the NMG.

Currently, most of the relevant studies are made for distributed control strategies in MGs without time delays [9]-[13]. Obviously, these distributed control strategies can achieve reasonable power distribution among ESSs, maintain the state of charge (SOC) balance, and restore the bus voltage deviation resulting from droop control in MGs. Note that a communication network is required for the distributed control of the NMG system. Additionally, the communication delays resulting from factors such as communication distance, channel noise become a significant influencing factor

Manuscript received: August 2, 2023; revised: December 2, 2023; accepted: April 28, 2024. Date of CrossCheck: April 28, 2024. Date of online publication: May 23, 2024.

This work was supported in part by the National Key Research and Development Program of China (No. 2018YFA0702200), the National Natural Science Foundation of China (No. 52377079), the Liaoning Revitalization Talents Program of China (No. XLYC2007181), and the Fundamental Research Funds for the Central Universities (No. N2204010).

G. Jing, B. Huang (corresponding author), R. Wang, and Q. Sun are with the School of Information Science and Engineering, Northeastern University, Shenyang 110819, China (e-mail: jingguoxiu512@163. com; huangbonan@ise. neu.edu.cn; wangrui@ise.neu.edu.cn; sunqiuye@ise.neu.edu.cn).

C. Yang is with the Information and Communication Branch, State Grid Liaoning Electric Power Company Ltd., Shenyang 110004, China (e-mail: yangchaoneu@sina.com).

DOI: 10.35833/MPCE.2023.000533

in the design of distributed consistency controllers [18]-[25]. According to [26]-[30], the communication delay significantly impacts the performance of the consistency control, leading to a significant deviation between the convergence value and the true value. In practical MG, a significant communication delay may not only result in bus voltage oscillations but also lead to system instability [18], [20], [33]-[37]. References [31] and [32] focus on the system with single type of time delay. Additionally, there are numerous works that concentrate on stability analysis of system with multiple types of time delays. For example, [34] presents a hierarchical control of the system with multiple types of time delays, while [38] and [40] present distributed control of the system with multiple time delays. Additionally, the stability of the system under load frequency control with multiple types of time delays is analyzed [39]. However, there is limited study on control methods of the NMG that simultaneously consider state delay, input delay, and communication delay, which poses a significant challenge.

The time delay is an inherent feature of the NMG. The distributed control method of the NMG relies on information exchange between MGs and HESUs, which inevitably causes time delay. Typically, time delay includes state, input, and communication delay, all of which affect the stability of the NMG [28]-[30]. In practical scenarios, the convergence of the NMG remains unaffected by communication delay, but it does impact the dynamic performance of the NMG, specifically resulting in a longer convergence time. However, the consistency convergence of the system is closely related to the input delay but independent of the communication delay. When the system parameters remain unchanged, a significant input delay can lead to system divergence and hinder the convergence of system consistency [30]-[32]. It is reported that most of the existing studies on the consistency problem in MG does not consider time delays, especially state delays. However, not all state variables can be measured in the NMG. The presence of multiple types of time delays can significantly reduce system stability and even result in system instability [20]. Furthermore, the multiple types of time delays in the NMG have an impact on system stability and make the design of control strategies of the NMG more challenging. Therefore, investigating the stability of the NMG with multiple types of time delays poses a new challenge that awaits breakthroughs.

Based on the above analysis, the fundamental issue faced by the NMG with multiple types of time delays is to improve the system stability and mitigate the influence of the time delays on system dynamic performance. The main control goal of the NMG is to proportionally distribute power according to the SOC of the HESUs, while simultaneously regulating the voltage of the point of common coupling (PCC) bus to the designed value. To achieve this goal, a distributed voltage control (DVC) strategy based on an observer is designed in this paper. Therein, the power controller of the DVC can ensure the SOC balance of the NMG while preventing over-charging and over-discharging of each HESU. However, the voltage controller of the DVC is based on an observer, and its control performance is influenced by both the initial value of the observer and time delays, which do not explicitly address time delays in the NMG. To address this issue, a state feedback control (SFC) strategy based on nested predictor is proposed to further mitigate the influence of time delays in the NMG. By actively compensating for input delay and communication delay, the proposed SFC strategy can improve the performance, responsiveness, and stability of the NMG. It provides a proactive solution to addressing the time delays of the NMG, which can minimize the adverse effects caused by these delays. Moreover, since the NMG with multiple types of time delays belongs with the complex network system, we analyze the large signal stability of the NMG at a systemic level. Based on this analysis, we assess the convergence and robustness of the proposed SFC strategy. Compared with the existing studies [14], [15], and [37], the proposed SFC strategy can actively compensate for time delays in the NMG system instead of passively tolerating them, resulting in higher reliability and robustness. The main contributions are summarized as follows.

1) Inspired by [33], an SFC strategy is proposed to mitigate the influence of multiple types of time delays in the NMG. To our knowledge, there are few studies on control methods for the NMG that simultaneously consider state delay, input delay, and communication delay, which poses a significant challenge.

2) Compared with the previous studies, the proposed SFC strategy requires neither the precise information from the communication network, nor the input signals between the HESUs. This strategy can achieve consensus control of the HESUs in the NMG and meet the requirements for SOC balance. Additionally, it regulates the voltage of the PCC bus in the NMG to its rated value. Moreover, the large-signal stability of the NMG is analyzed at a systemic level.

3) The proposed SFC strategy can actively compensate for both input delay and communication delay. Furthermore, the NMG can effectively resist the impact of multiple types of time delays, which has higher reliability and robustness.

The summary of the remaining content in this paper is provided as follows. The architecture of the NMG with HESUs is presented in Section II. Section III constructs the proposed SFC strategy to mitigate the influence of multiple types of time delays, then analyzes the stability of the closed-loop NMG. Experimental results demonstrate the reliability and robustness of the proposed SFC strategy in Section IV. Finally, the overall conclusion is summarized in Section V.

II. Architecture of NMG with HESUs

A. Cyber-physical Architecture of NMG

In an islanded NMG, the randomness and intermittency of the DERs cannot guarantee a stable energy output. Therefore, HESUs are necessary to compensate for the unbalanced power between photovoltaic (PV) power generation and load, as well as to stabilize the bus voltage. Figure 1 presents the configuration of the NMG with HESUs. The MG mainly consists of RESs, distributed HESUs, and DC loads. The HESUs should ensure that the SOC of each HESU is balanced to avoid over-charging and over-discharging prob-

lems. Multiple HESUs are controlled by connecting bidirectional DC/DC converters to form the DERs. The PV system of the NMG can fully harness the potential of alternative energy sources through its maximum power point tracking (MPPT) operation mode, which does not participate in distributed control among HESUs. Furthermore, HESUs are utilized to regulate the voltage of the PCC bus in the NMG and address the issue of randomness on both power side and load side.

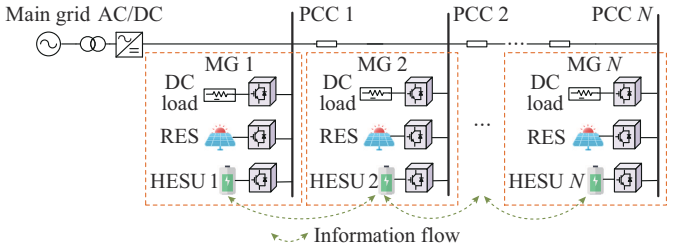

Fig. 1. Configuration of NMG with HESUs.

This paper considers the communication network of the NMG with N HESUs, which is modeled as a directed graph $\bar{\mathcal{G}}=(\mathcal{V},\mathcal{E},\mathcal{G})$, where $\mathcal{V}=\{1,2,\ldots,N\}$ is the set of N HESUs in the NMG; and $\mathcal{E}\in\mathcal{V}\times\mathcal{V}$ is the edge set of N HESUs. According to graph theory in [36], $\mathcal{G}=\{\mathcal{G}_{ij}\}$ is the set of communication weights between adjacent nodes, where $\mathcal{G}_{ij}\in\mathcal{V}$ is the non-negative element. In the cyber layer of the NMG, $\mathcal{E}$ is the connection between the i^{th} HESU and the j^{th} HESU. The assumption implies that $\mathcal{G}_{ii}=0$ for all $i\in\mathcal{E}$, and $\mathcal{G}_{ij}>0$ only if $(i,j)\in\mathcal{E}$. $\boldsymbol{L}$ is introduced to describe the Laplacian matrix of the NMG, which is also defined in [36], and we have $L_{ii}=-\sum_{j=1}^{N}L_{ij}$, where $L_{ij}=-\mathcal{G}_{ij}$, $i\neq j$, and $\sum_{j=1}^{N}L_{ij}=0$. It is worth noting that the directed graph provides a simplification and abstraction, which helps better understand the structure and behavior of the NMG.

B. SOC Balance of HESUs

The SOC in the NMG indicates the residual capacity of HESUs, which is a crucial metric for assessing the charging and discharging of HESUs. Considering the existence of different initial values of SOC among HESUs and the influence of ambient temperature on line resistance, it is necessary to maintain the SOC balance of HESUs during the charging and discharging process. The SOC balance control proposed in [37] can prevent over-discharging and over-charging of some HESUs, thereby enhancing the lifespan of the battery. Based on the Coulomb counting technique, the SOC of HESUs can be accurately acquired, which is obtained as:

$$SOC_i=SOC_i(0)-\frac{1}{C_{HESUi}}\int i_{HESUi}\,\mathrm{d}t \tag{1}$$

where SOC_i is the current SOC of the i^{th} HESU; $SOC_i(0)$ is the initial SOC of the i^{th} HESU; i_{HESUi} is the output current of the i^{th} HESU; and C_{HESUi} is the rated capacity of the i^{th} HESU.

The power loss of the converters is disregarded for the HESUs, and it is assumed that the charging and discharging efficiency as well as the port voltage remains constant. Then, we can further obtain:

$$SOC_i=SOC_i(0)-\frac{1}{C_{HESUi}}\int\frac{P_{HESUi}}{U_{HESUi}}\,\mathrm{d}t \tag{2}$$

where P_{HESUi} is the output power of the i^{th} HESU; and U_{HESUi} is the output voltage of the i^{th} HESU.

Note that the SOC balance of HESUs is directly controlled, which may result in charging and discharging as well as circulation among HESUs. To address this issue, define the state variable of the power allocation and then couple the output power to the SOC through this state variable. Furthermore, we incorporate SOC information into the controllers of the NMG to achieve the SOC balance of HESUs. The defined state variable can be expressed as:

$$\delta_i=\frac{P_{HESUi}}{F(SOC_i)} \tag{3}$$

where $F(SOC_i)$ is the actual remaining available capacity of the i^{th} HESU; and δ_i is the power allocation variable.

$$F(SOC_i)=\begin{cases}C_{HESUi}(SOC_i-SOC_{\text{L}}) & \text{discharging state}\\ C_{HESUi}(SOC_{\text{H}}-SOC_i) & \text{charging state}\end{cases} \tag{4}$$

where $SOC_{\text{L}}=0.2$ is the lower bound of SOC in discharging state; and $SOC_{\text{H}}=0.8$ is the upper bound of SOC in charging state.

Remark 1: it should be noted that the state variable ensures simultaneous charging and discharging of all HESUs in the NMG, while adjusting the output power according to residual power, so that the SOC of HESUs gradually converges to the same value. Meanwhile, the unbalanced power will be allocated among HESUs based on the real-time state of SOC when the state variables of the HESUs become consistent.

C. Primary Control of HESUs

For an islanded NMG, the traditional droop control method is applied to achieve power sharing among HESUs. Then, the steady-state expression can be obtained as:

$$V_{PCCi}=V_{\text{refi}}^{*}-r_{HESUi}i_{HESUi} \tag{5}$$

where V_{PCCi} is the voltage of the PCC bus of the i^{th} HESU; V_{refi}^{*} is the reference voltage of the PCC bus of the i^{th} HESU, which is modified by the distributed secondary control; and r_{HESUi} is the droop coefficient of the primary control of the i^{th} HESU.

The power sharing ratio is defined as inversely proportional to r_{HESUi}. Then, it can be obtained that:

$$r_{HESUi}=\frac{V_{nom}-V_{\min}}{P_{nomi}}=\frac{V_{\max}-V_{nom}}{P_{nomi}} \tag{6}$$

where $V_{\max}$ and $V_{\min}$ are the maximum and minimum offset voltages of the PCC bus in the NMG, respectively; V_{nom} is the nominal voltage of the PCC bus; and P_{nomi} is the nominal power of the i^{th} HESU.

According to (5) and (6), it is observed that accurate power sharing among HESUs can be achieved if the droop coefficient is sufficiently large. However, this will result in significant voltage deviation at the steady state. Thus, the droop coefficient of the HESUs can be restricted to:

$$0<r_{HESUi}\leq r_{HESUi}^{\max}=\frac{\Delta U_{\max}}{I_i^{nom}} \tag{7}$$

where $r_{HESUi}^{\max}$ is the upper limit of r_{HESUi}; I_i^{nom} is the nominal current of the i^{th} HESU; and $\Delta U_{\max}$ is the maximum allowable voltage deviation of PCC bus.

Remark 2: for an islanded NMG, due to the different capacities and line resistances of HESUs, it is a challenge for HESUs to achieve SOC balance and accurate power allocation with multiple types of time delays. Furthermore, it is necessary to avoid over-charging and over-discharging when the power allocation of HESUs is consistent with the SOC. However, the voltage deviation in the NMG and the presence of line impedance can inevitably result in imprecise power allocation among HESUs. Thus, it is imperative to redesign the control strategy for the NMG.

III. Proposed Control Strategy

A. Proposed DVC Strategy

The proposed DVC strategy is illustrated in Fig. 2. The control structure mainly includes a power controller, a voltage controller, and a voltage observer. The main challenges to be addressed in the droop control of the NMG are the steady-state voltage deviation and accuracy in power allocation. On one hand, the voltage controller calculates the error between the designed nominal voltage and the observed voltage, and then inputs this error value into the proportional-integral (PI) controller to obtain the voltage adjustment term Δu_{HESU}. On the the other hand, the power allocation variable δ_i of HESUs exchanges information to obtain error signal $\Delta e = -\sum_{j=1}^{N} a_{ij}(\delta_i - \delta_j)$, and then inputs the error value into the power controller to obtain the power adjustment term Δp_{HESU}. Finally, the two adjustment terms are added to the droop controller to produce a fresh value V_{refi}^* for reference voltage of the primary controller. The control objective is to adjust the average voltage of the PCC bus in the NMG to its designed nominal value.

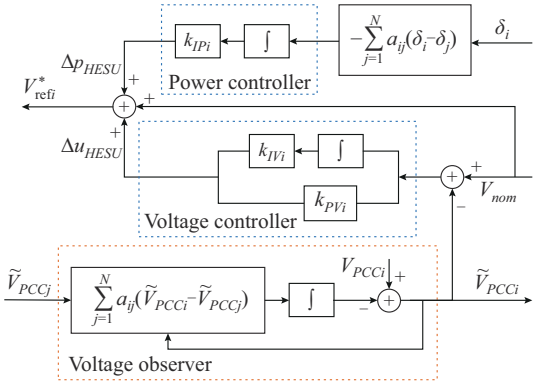

Fig. 2. Structure of proposed DVC strategy.

The nominal voltage of the PCC bus can be expressed as:

$$\frac{1}{N}\sum_{i=1}^{N} V_{PCCi} = V_{nom} \tag{8}$$

The voltage observer of the secondary control is given as:

$$\tilde{V}_{PCCi} = V_{PCCi} - \int \sum_{j=i}^{N} a_{ij}(\tilde{V}_{PCCi} - \tilde{V}_{PCCj})\mathrm{d}t \tag{9}$$

where $\tilde{V}_{PCCi}$ and $\tilde{V}_{PCCj}$ are the average voltages of the PCC bus of the i^{th} and the j^{th} HESUs, respectively, which are captured by the voltage observer.

The modified droop control with the voltage adjustment term is designed as:

$$V_{\text{refi}}^* = V_{nom} - \Delta v_i + \Delta u_i \tag{10}$$

where Δu_i is the compensation required for bus voltage recovery provided by the distributed secondary control of the i^{th} HESU; and Δv_i is the voltage decrease resulting from the droop control.

Next, according to (8), it can be obtained that:

$$\Delta u_i = \Delta u_{HESU} + \Delta p_{HESU} \tag{11}$$

In addition, the voltage decrease resulting from the implementation of droop control can be expressed as:

$$\Delta v_i = r_{HESUi} i_{HESUi} \tag{12}$$

Note that the power sharing ratio of the HESU is defined to be inversely proportional to r_{HESUi}. Then, we have the following conditions:

$$\Delta v_1 = \Delta v_2 = \ldots = \Delta v_N \tag{13}$$

To obtain the voltage adjustment term of the PCC bus, the error between the designed nominal voltage and the observed voltage is calculated, and the output error is then inputted into the PI controller for regulation, as shown in (9).

$$\Delta u_{HESU} = k_{PVi}(V_{nom} - \tilde{V}_{PCCi}) + k_{IVi}(V_{nom} - \tilde{V}_{PCCi}) \tag{14}$$

where k_{PVi} is the designed proportional coefficient for the voltage controller of the NMG; and k_{IVi} is the designed integral coefficient for the voltage controller of the NMG.

In the communication network layer of the NMG, the power allocation variable δ_i of each HESU exchanges information to obtain the error signal Δe, and inputs the error value into the power controller to acquire the power adjustment term.

$$\Delta p_{HESU} = -k_{IPi}\sum_{j=1}^{N} a_{ij}(\delta_i - \delta_j) \tag{15}$$

where k_{IPi} is the integral coefficient of power controller.

Remark 3: it should be noted that in the case where the variables δ_i of the HESUs are not identical, the power controller will make necessary adjustments to account for the error. Each HESU needs to continuously monitor the reference voltage of the PCC bus in real time until all HESUs converge to the same value. Furthermore, by utilizing the voltage observer described in (9), HESUs can exchange information and iterate to obtain a consistent average voltage observation value. Based on this, the HESUs have the ability to promptly adapt to power variations in the NMG, thereby ensuring a proportional relationship between output power and SOC of the HESUs. Moreover, the voltage of the PCC bus in the NMG can be adjusted to the rated value.

B. Constructed SFC Strategy with Multiple Types of Time Delays

The existence of the state delay, input delay, and asymmetric communication delay in the NMG can affect control performance and may even lead to voltage oscillation on the PCC bus and system instability. In this subsection, the aim of this paper is to propose a control strategy that enhances

the stability of the NMG with multiple types of time delays and mitigates their impacts on the dynamic performance of the system. However, due to the time delays in the NMG and the influence of the initial observer value, the estimation of the proposed DVC strategy is not accurate enough for adjusting the average voltage of the PCC bus to the nominal value. According to [33], the problem of the state delay and input delay is addressed by constructing a feedback controller based on nested predictors. Inspired by the idea in [33], an SFC strategy based on nested predictors is proposed to predict future state information, which can mitigate the influence of time delays in the NMG. Moreover, the input delay and communication delay can be fully compensated. Since the nested predictor can recursively obtain future state information with a step size, the state delay is equivalent to the step size and can also be addressed.

The designed controller of the NMG in this paper mainly includes primary control and distributed secondary control with cyber layer. The structure of the proposed SFC strategy is shown in Fig. 3, where the primary control is mainly divided into droop control and voltage and current control. The distributed secondary control can eliminate the error by adjusting the offset of the droop control in the NMG. In addition, variables V_{PCCi} and δ_i, required for the distributed secondary control are exchanged in the cyber layer. Among them, the state variable δ_i couples the output power of the HESUs with the SOC. The aim of this paper is to achieve precise power allocation among HESUs in the NMG and restore the voltage of the PCC bus to the nominal voltage.

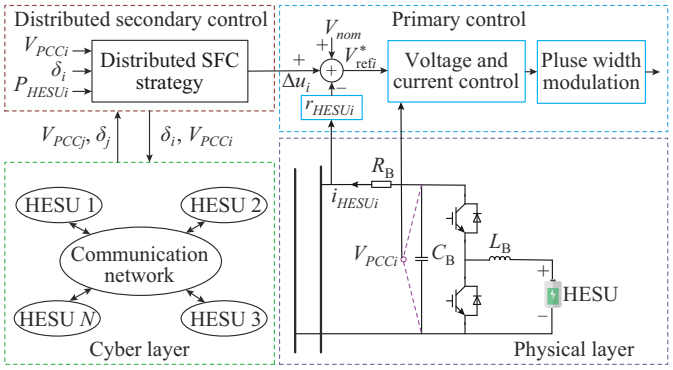

Fig. 3. Structure of proposed SFC strategy.

Definition of the consensus in the NMG: considering a communication network of an NMG with N HESUs modeled by a directed graph $\bar{\mathcal{G}}$, the proposed SFC strategy can ensure that the HESUs can achieve consensus if

$$\lim_{t\to\infty}\|\boldsymbol{x}_i(t)-\boldsymbol{x}_j(t)\|=0 \quad i,j=1,2,...,N \tag{16}$$

where $\boldsymbol{x}_i(t)$ and $\boldsymbol{x}_j(t)$ are the state vectors of the i^{th} and the j^{th} HESUs at time t, respectively.

It is assumed that the HESUs in the NMG broadcast information through a directed communication network, which means that the topology of the NMG contains a directed spanning tree [15]. Therefore, $\lim_{t\to\infty}(\tilde{V}_{PCCi}-\tilde{V}_{PCCj})=0$, which denotes that the voltages of all PCC buses converge to the arithmetic mean value, i.e., $\lim_{t\to\infty}\tilde{V}_{PCCi}=\frac{1}{N}\lim_{t\to\infty}V_{PCCi}$.

Inspired by the concept of the consensus algorithm, for the NMG without common bus, it is meaningful to propose a control strategy that ensures the gradual convergence of the average voltage of PCC buses towards its designed nominal value. Furthermore, we aim to propose an SFC strategy to address the consensus issue of HESUs in the NMG.

Considering the discrete form of the NMG with N HESUs, we can obtaion:

$$\boldsymbol{x}_i(t+1)=\boldsymbol{A}\boldsymbol{x}_i(t)+\boldsymbol{A}_r\boldsymbol{x}_i(t-r)+\boldsymbol{B}\boldsymbol{u}_i(t-h) \quad i=1,2,...,N \tag{17}$$

where $\boldsymbol{u}_i(t)$ is the control vector of the i^{th} HESU at time t; r is the state delay that occurs in the data sampling process from sensors to the controller in the NMG, $r\geq 1$; h is the input delay, which refers to the time delay between sending a control signal from the controller to the actuator and the subsequent response of the actuator in the NMG, $h\geq 1$; and $\boldsymbol{A}$, $\boldsymbol{B}$, and $\boldsymbol{A}_r$ are constant matrices.

Note that voltage deviations occur in the NMG due to the line impedances and device losses. Therefore, the proposed SFC strategy can further enhance the tracking accuracy. For the considered NMG in (17), the i^{th} HESU captures the state variable data of its adjacent HESUs $\boldsymbol{z}_i(t+k)$ for the feedback at time t, and then captures the input variable data of its adjacent HESUs $\boldsymbol{v}_i(t+s)$ for feedback, where $k=-d_i-N, -d_i-N+1,...,-d_i$, $s=-N,-N+1,...,-1$; and $d_i\geq 1$ is the communication delay among HESUs, which is given integers.

$\boldsymbol{z}_i(t)$ is the state feedback function at time t, which can be expressed as:

$$\boldsymbol{z}_i(t)=\sum_{j=1}^{N}\mathcal{G}_{ij}(\boldsymbol{x}_i(t)-\boldsymbol{x}_j(t))=\sum_{j=1}^{N}L_{ij}\boldsymbol{x}_j(t) \tag{18}$$

$\boldsymbol{v}_i(t)$ is also the state feedback function, which can be expressed as:

$$\boldsymbol{v}_i(t)=\sum_{j=1}^{N}\mathcal{G}_{ij}(\boldsymbol{u}_i(t)-\boldsymbol{u}_j(t))=\sum_{j=1}^{N}L_{ij}\boldsymbol{u}_j(t) \tag{19}$$

Assumption 1: the directed network $\bar{\mathcal{G}}=(\mathcal{V},\mathcal{E},\mathcal{G})$ of the NMG is balanced and connected, which includes a directed spanning tree constructed with the reference signals of the HESUs as the root node.

Based on [36], set a matrix $\bar{\boldsymbol{\Phi}}\in\mathbf{R}^{N\times N}$ as nonsingular matrix, which is given by:

$$\bar{\boldsymbol{\Phi}}^{-1}\boldsymbol{L}\bar{\boldsymbol{\Phi}}=\begin{bmatrix}0&0&0&0&\cdots&0\\0&\lambda_2&\partial_2&0&\cdots&0\\0&0&\lambda_3&\partial_3&\cdots&0\\\vdots&\vdots&\vdots&\vdots&\cdots&\vdots\\0&0&0&0&\cdots&\lambda_N\end{bmatrix}\triangleq\boldsymbol{J}_L \tag{20}$$

where $\partial_i\in\{0,1\}$ for $i=2,3,...,N-1$, and $\partial_N=0$; and λ_i is the eignvalue of $\boldsymbol{L}$. The eigenvalues of $\boldsymbol{L}$ are expressed as λ_i, $i=2,3,...,N$; and $\mathbf{1}_N\triangleq[1,\ 1,\ ...,1]^{\mathrm{T}}$ is the first column of the nonsingular matrix $\bar{\boldsymbol{\Phi}}$.

It can be observed from Assumption 1 that $\mathrm{Re}(\lambda_i)>0$, $i=2,3,...,N$. In addition, the consensus of HESUs in the NMG can also be achieved without time delay. The proposed SFC strategy is defined as:

$$\boldsymbol{u}_i(t)=\boldsymbol{F}(\boldsymbol{z}_i(t+k))+\boldsymbol{H}(\boldsymbol{v}_i(t+s)) \quad i=1,2,...,N \tag{21}$$

where $\boldsymbol{F}(\cdot)$ and $\boldsymbol{H}(\cdot)$ are the linear operators.

Then, we impose another assumption in the NMG.

Assumption 2: matrix $\boldsymbol{K}\in\mathbf{R}^{m\times n}$ and matrix $\boldsymbol{K}_r\in\mathbf{R}^{m\times n}$ can ensure the asymptotic stability of the NMG with the following series of time delay.

$$\bar{\boldsymbol{\chi}}_i(t+1)=(\boldsymbol{A}+\lambda_i\boldsymbol{B}\boldsymbol{K})\bar{\boldsymbol{\chi}}_i(t)+(\boldsymbol{A}_r+\lambda_i\boldsymbol{B}\boldsymbol{K}_r)\bar{\boldsymbol{\chi}}_i(t-r) \tag{22}$$

where $\overline{(\cdot)}$ represents the dynamics of the corresponding variables.

Based on [33], we can obtain the gain matrices $\boldsymbol{K}$ and $\boldsymbol{K}_r$ for feedback by using the linear matrix inequality (LMI) technique. Next, Lemma 1 is presented to provide an explanation for the above assumption.

Lemma 1: consider a high-order discrete-time NMG that exclusively incorporates the state delays:

$$\bar{\boldsymbol{x}}_i(t+1)=\boldsymbol{A}\bar{\boldsymbol{x}}_i(t)+\boldsymbol{A}_r\bar{\boldsymbol{x}}_i(t-r)+\boldsymbol{B}\bar{\boldsymbol{u}}_i(t) \tag{23}$$

Assume that the i^{th} HESU captures the state variable data of its adjacent HESUs for feedback at time t.

$$\bar{\boldsymbol{z}}_i(t)=\sum_{j=1}^{N}\mathcal{G}_{ij}(\bar{\boldsymbol{x}}_i(t)-\bar{\boldsymbol{x}}_j(t))=\sum_{j=1}^{N}L_{ij}\bar{\boldsymbol{x}}_j(t) \tag{24}$$

Then, only if Assumption 2 is fulfilled, the following SFC protocol can achieve the consensus among the HESUs in the NMG. The compact form of the feedback SFC protocol is expressed as:

$$\bar{\boldsymbol{u}}_i(t)=\boldsymbol{K}\bar{\boldsymbol{z}}_i(t)+\boldsymbol{K}_r\bar{\boldsymbol{z}}_i(t-r)\quad i=1,2,...,N \tag{25}$$

Lemma 2: suppose that the NMG in (22) can achieve asymptotic stability with multiple types of time delays, if there exist the matrices $\boldsymbol{P}>\boldsymbol{0}$ and $\boldsymbol{Q}>\boldsymbol{0}$. Furthermore, there are also matrices $\boldsymbol{U}$ and $\boldsymbol{U}_r$ satisfying the LMI, and λ_i^* is introduced to denote the conjugate number of λ_i.

$$\begin{bmatrix}\boldsymbol{Q}-\boldsymbol{P} & \boldsymbol{0} & \boldsymbol{P}\boldsymbol{A}^{\mathrm{T}}+\lambda_i^*\boldsymbol{U}^{\mathrm{T}}\boldsymbol{B}^{\mathrm{T}}\\ \boldsymbol{0} & -\boldsymbol{Q} & \boldsymbol{P}\boldsymbol{A}_r^{\mathrm{T}}+\lambda_i^*\boldsymbol{U}_r^{\mathrm{T}}\boldsymbol{B}^{\mathrm{T}}\\ \boldsymbol{A}\boldsymbol{P}+\lambda_i\boldsymbol{B}\boldsymbol{U} & \boldsymbol{A}_r\boldsymbol{P}+\lambda_i\boldsymbol{B}\boldsymbol{U}_r & -\boldsymbol{P}\end{bmatrix}<\boldsymbol{0} \tag{26}$$

Based on [33], the matrices $\boldsymbol{K}$ and $\boldsymbol{K}_r$ can be designed as:

$$\begin{cases}\boldsymbol{K}=\boldsymbol{U}\boldsymbol{P}^{-1}\\ \boldsymbol{K}_r=\boldsymbol{U}_r\boldsymbol{P}^{-1}\end{cases} \tag{27}$$

To achieve consensus among the HESUs in the NMG, an SFC protocol based on a predictor is designed as:

$$\boldsymbol{u}_i(t)=\boldsymbol{K}\boldsymbol{z}_i(t+h)+\boldsymbol{K}_r\boldsymbol{z}_i(t+h-r) \tag{28}$$

The detailed design steps of the predictor are then provided. Specifically, we let:

$$\tau_i=h+d_i\quad i=1,2,...,N \tag{29}$$

Thus, we can predict that:

$$\boldsymbol{z}_i(t+h)=\boldsymbol{A}\boldsymbol{z}_i(t)+\boldsymbol{A}_r\boldsymbol{z}_i(t-r)+\boldsymbol{B}\boldsymbol{v}_i(t-h) \tag{30}$$

Next, through the prediction of $\boldsymbol{z}_i(t+h)$, we can obtain:

$$\hat{\boldsymbol{z}}_i(t+h)=\boldsymbol{A}^{\tau_i}\boldsymbol{z}_i(t-d_i)+\sum_{l=0}^{\tau_i-1}\boldsymbol{A}^{\tau_i-1-l}\boldsymbol{A}_r\boldsymbol{z}_i(t-d_i-r+l)+\sum_{l=0}^{\tau_i-1}\boldsymbol{A}^{\tau_i-1-l}\boldsymbol{B}\boldsymbol{v}_i(t-\tau_i+l) \tag{31}$$

where $\hat{\boldsymbol{z}}_i(s)$ $(s>0)$ is the predicted value of $\boldsymbol{z}_i(s)$, and if $s\le 0$, $\hat{\boldsymbol{z}}_i(s)=\boldsymbol{z}_i(s)$.

If $\tau_i\le r+1$, $\hat{\boldsymbol{z}}_i(t+h)$ is a causal system and therefore can be implemented. Nonetheless, in the event that $\tau_i>r+1$, $\boldsymbol{A}^{\tau_i-1-l}\boldsymbol{A}_r\boldsymbol{z}_i(t-d_i-r+l)$ continues to rely on the next state data $\boldsymbol{z}_i(t+s)$, $s\in(-d_i,h-r-1]$. It should be noted that this designed predictor cannot achieve the control objective of the NMG under Assumption 2. Since the obtained protocol depends on future states, the predictors are acausal and therefore cannot be implemented.

Hence, to address the above issue, we assume that:

$$\tau_i>r+1 \tag{32}$$

To attain the control objective, it is noted that all types of time delays in the NMG can be unified in (32). Besides, there exist integers ρ_i and r_i, $1\le r_i\le r$ such that:

$$\rho_i r+r_i=\tau_i \tag{33}$$

Inspired by [33], a nested predictor is designed to address the above issues. The primary concept is explained in the following steps.

Step 1: predicting $\boldsymbol{z}_i(t-d_i+\theta_1)$ $(\theta_1=1,2,...,r)$ from (30), it can be obtained that:

$$\hat{\boldsymbol{z}}_i(t-d_i+\theta_1)=\boldsymbol{A}^{\theta_1}\boldsymbol{z}_i(t-d_i)+\sum_{l=0}^{\theta_1-1}\boldsymbol{A}^{\theta_1-1-l}\boldsymbol{B}\boldsymbol{v}_i(t-\tau_i+l)+\sum_{l=0}^{\theta_1-1}\boldsymbol{A}^{\theta_1-1-l}\boldsymbol{A}_r\boldsymbol{z}_i(t-d_i-r+l) \tag{34}$$

When $\boldsymbol{z}_i(t+k)$ is with $\boldsymbol{v}_i(t+k)$, it can be found that $\boldsymbol{z}_i(t-d_i+\theta_1)$ is a causal system and therefore can be implemented.

Step 2: using the previous predicted value $\hat{\boldsymbol{z}}_i(t-d_i+\theta_1)$ $(\theta_1=1,2,...,r)$ and $\boldsymbol{v}_i(t+s)$ $(s=-N,-N+1,\ldots,-1)$ to predict $\hat{\boldsymbol{z}}_i(t-d_i+r+\theta_2)$ $(\theta_1=1,2,...,r)$, it can be obtained that:

$$\hat{\boldsymbol{z}}_i(t-d_i+r+\theta_2)=\boldsymbol{A}^{\theta_2}\hat{\boldsymbol{z}}_i(t-d_i+r)+\sum_{l=0}^{\theta_2-1}\boldsymbol{A}^{\theta_2-1-l}\boldsymbol{A}_r\hat{\boldsymbol{z}}_i(t-d_i+l)+\sum_{l=0}^{\theta_2-1}\boldsymbol{A}^{\theta_2-1-l}\boldsymbol{B}\boldsymbol{v}_i(t+r-\tau_i+l) \tag{35}$$

We can use state variable value $\boldsymbol{z}_i(t-d_i+(j-1)r+\theta_j)$ $(\theta_j=1,2,...,r)$ and $\boldsymbol{v}_i(t+s)$ $(s=-N,-N+1,\cdots,-1)$ to predict $\boldsymbol{z}_i(t-d_i+jr+\theta_{j+1})$ for $j=1,2,...,\rho_i-1$ and $\theta_j=1,2,...,r$. Then, we can obtain that:

$$\hat{\boldsymbol{z}}_i(t-d_i+jr+\theta_{j+1})=\boldsymbol{A}^{\theta_{j+1}}\hat{\boldsymbol{z}}_i(t-d_i+jr)+\sum_{l=0}^{\theta_{j+1}-1}\boldsymbol{A}^{\theta_{j+1}-1-l}\boldsymbol{A}_r\hat{\boldsymbol{z}}_i(t-d_i+(j-1)r+l)+\sum_{l=0}^{\theta_{j+1}-1}\boldsymbol{A}^{\theta_{j+1}-1-l}\boldsymbol{B}\boldsymbol{v}_i(t+jr-\tau_i+l) \tag{36}$$

It can be found that $\boldsymbol{z}_i(t-d_i+jr+\theta_{j+1})$ is a causal system, which can therefore be implemented.

Step 3: when $\theta_{\rho_i+1}=1,2,...,r_i$, we have:

$$\hat{\boldsymbol{z}}_i(t-d_i+\rho_i r+\theta_{\rho_i+1})=\boldsymbol{A}^{\theta_{\rho_i+1}}\hat{\boldsymbol{z}}_i(t-d_i+\rho_i r)+\sum_{l=0}^{\theta_{\rho_i+1}-1}\boldsymbol{A}^{\theta_{\rho_i+1}-1-l}\boldsymbol{A}_r\hat{\boldsymbol{z}}_i(t-d_i+(\rho_i-1)r+l)+\sum_{l=0}^{\theta_{\rho_i+1}-1}\boldsymbol{A}^{\theta_{\rho_i+1}-1-l}\boldsymbol{B}\boldsymbol{v}_i(t+\rho_i r-\tau_i+l) \tag{37}$$

Then, the restructured proposed SFC protocol based on a predictor is expressed as:

$$\boldsymbol{u}_i(t)=\boldsymbol{K}\hat{\boldsymbol{z}}_i(t+h)+\boldsymbol{K}_r\hat{\boldsymbol{z}}_i(t+h-r)\quad i=1,2,...,N \tag{38}$$

$\hat{\boldsymbol{z}}_i(t+\bar{s})$, $\bar{s}=-d_i,-d_i+1,...,h$ can be obtained by (37). In this way, we can predict $\hat{\boldsymbol{z}}(t+\tau_i)$ as the step size with any integer $\delta=1,2,...,r$.

Remark 4: the feedback controller proposed in this paper is based on a nested predictor with SFC protocol. It should be noted that the SFC protocol is structurally independent of the proposed feedback controller. Equation (17) provides the definition of state delay and input delay. The control input $\boldsymbol{u}_i(t)$ in (17) employs linear mapping, and the proposed SFC strategy in (21) provides the definition of communication delay. Furthermore, all types of time delays can be unified in the SFC protocol, which can be observed in (32) of the nested prediction step. By implementing the SFC protocol in (27) along with (18) and (19), the distributed consensus of the NMG with N HESUs in (17) can be achieved through the feedback process in (32)-(37). Moreover, the input delay and communication delay can be fully compensated. Since the nested predictor obtains future state information recursively with a step size, the state delay is equivalent to the step size and can also be addressed.

Remark 5: it should be noted that the proposed SFC strategy can recursively obtain future state information of the NMG with a step size of r. In this subsection, the capacity difference of the HESUs, the mismatch of the corresponding line resistance, and the existence of time delays in the NMG are considered. However, these factors may hinder the guarantee of SOC balance of the HESUs and accurate power allocation. The theoretical analysis indicates that the proposed SFC strategy can achieve precise power distribution at the steady state of the NMG with multiple types of time delays.

C. Stability Analysis

We transform the stability of the NMG consisting of (17) and (36) into the stability analysis presented in (22). Theorem 1 and its proof are established to guarantee the consensus of HESUs in the NMG with multiple types of time delays.

Theorem 1: suppose that Assumptions 1 and 2 are satisfied. The consensus of the HESUs in the NMG in (17) can be achieved.

Proof: considering (18), (19), and (37), $\boldsymbol{u}_i(t)$ can be rewritten as:

$$\begin{aligned}\boldsymbol{u}_i(t)=&\boldsymbol{K}\sum_{j=1}^{N}L_{ij}\boldsymbol{x}_j(t-d_i+\rho_i r+\theta_{\rho_i+1})+\\&\boldsymbol{K}_r\sum_{j=1}^{N}L_{ij}\boldsymbol{x}_j(t-d_i+(\rho_i-1)r+\theta_{\rho_i+1})\end{aligned}\tag{39}$$

$$\begin{aligned}\boldsymbol{x}_j(t-d_i+\rho_i r+\theta_{\rho_i+1})=&\boldsymbol{A}^{\theta_{\rho_i+1}}\boldsymbol{x}_j(t-d_i+\rho_i r)+\\&\sum_{l=0}^{\theta_{\rho_i+1}-1}\boldsymbol{A}^{\theta_{\rho_i+1}-1-l}\boldsymbol{A}_r\boldsymbol{x}_j(t-d_i+(\rho_i-1)r+l)+\\&\sum_{l=0}^{\theta_{\rho_i+1}-1}\boldsymbol{A}^{\theta_{\rho_i+1}-1-l}\boldsymbol{B}\boldsymbol{u}_j(t+\rho_i r-\tau_i+l)\end{aligned}\tag{40}$$

Then, it follows (40) that:

$$\begin{aligned}\boldsymbol{\chi}(t-d_i+\rho_i r+\theta_{\rho_i+1})=&(\boldsymbol{I}_N\otimes\boldsymbol{A}^{\theta_{\rho_i+1}})\boldsymbol{\chi}(t-d_i+\rho_i r)+\\&\sum_{l=0}^{\theta_{\rho_i+1}-1}(\boldsymbol{I}_N\otimes\boldsymbol{A}^{\theta_{\rho_i+1}-1-l}\boldsymbol{A}_r)\boldsymbol{\chi}(t-d_i+(\rho_i-1)r+l)+\\&\sum_{l=0}^{\theta_{\rho_i+1}-1}(\boldsymbol{I}_N\otimes\boldsymbol{A}^{\theta_{\rho_i+1}-1-l}\boldsymbol{B})\boldsymbol{\mu}(t+\rho_i r-\tau_i+l)\end{aligned}\tag{41}$$

where $\otimes$ denotes the Kronecker product.

The variables $\boldsymbol{\chi}$ and $\boldsymbol{\mu}$ are defined as:

$$\begin{cases}\boldsymbol{\chi}\triangleq[\boldsymbol{\chi}_1^{\mathrm{T}},\boldsymbol{\chi}_2^{\mathrm{T}},\ldots,\boldsymbol{\chi}_N^{\mathrm{T}}]^{\mathrm{T}}\triangleq(\bar{\boldsymbol{\Phi}}^{-1}\otimes\boldsymbol{I}_n)\boldsymbol{x}\\\boldsymbol{\mu}\triangleq[\boldsymbol{\mu}_1^{\mathrm{T}},\boldsymbol{\mu}_2^{\mathrm{T}},\ldots,\boldsymbol{\mu}_N^{\mathrm{T}}]^{\mathrm{T}}\triangleq(\bar{\boldsymbol{\Phi}}^{-1}\otimes\boldsymbol{I}_n)\boldsymbol{u}\end{cases}\tag{42}$$

Then, we further define $\boldsymbol{Z}(f(t))$ as Z-transformation of $f(t)$, and the following fact can be obtained.

$$\begin{aligned}\boldsymbol{Z}(\boldsymbol{\chi}(t-d_i+\rho_i r+\theta_{\rho_i+1}))=&(\boldsymbol{I}_N\otimes\boldsymbol{A}^{\theta_{\rho_i+1}})z^{-d_i+\rho_i r}\boldsymbol{X}(z)+\\&\sum_{l=0}^{\theta_{\rho_i+1}-1}(\boldsymbol{I}_N\otimes\boldsymbol{A}^{\theta_{\rho_i+1}-1}\boldsymbol{B})z^{\rho_i r-\tau_i+l}\boldsymbol{U}(z)+\\&\sum_{l=0}^{\theta_{\rho_i+1}-1}(\boldsymbol{I}_N\otimes\boldsymbol{A}^{\theta_{\rho_i+1}-1-l}\boldsymbol{A}_r)z^{-d_i+(\rho_i-1)r+l}\boldsymbol{X}(z)\triangleq\\&\boldsymbol{F}(\rho_i,z)\boldsymbol{X}(z)+\boldsymbol{H}(\rho_i,z)(\boldsymbol{I}_N\otimes\boldsymbol{B})\boldsymbol{U}(z)\end{aligned}\tag{43}$$

$$\boldsymbol{F}(\rho_i,z)=(\boldsymbol{I}_N\otimes\boldsymbol{A}^{\theta_{\rho_i+1}})z^{-d_i+\rho_i r}+\sum_{l=0}^{\theta_{\rho_i+1}-1}(\boldsymbol{I}_N\otimes\boldsymbol{A}^{\theta_{\rho_i+1}-1-l}\boldsymbol{A}_r)z^{-d_i+(\rho_i-1)r+l}\tag{44}$$

$$\boldsymbol{H}(\rho_i,z)=\sum_{l=0}^{\theta_{\rho_i+1}-1}(\boldsymbol{I}_N\otimes\boldsymbol{A}^{\theta_{\rho_i+1}-1})z^{\rho_i r-\tau_i+l}\tag{45}$$

Based on (33), $\boldsymbol{\chi}(t+1)$ and $\boldsymbol{\mu}(t)$ can be represented as (46) and (47), respectively.

$$\boldsymbol{\chi}(t+1)=(\boldsymbol{I}_N\otimes\boldsymbol{A})\boldsymbol{\chi}(t)+(\boldsymbol{I}_N\otimes\boldsymbol{B})\boldsymbol{\mu}(t-h)+(\boldsymbol{I}_N\otimes\boldsymbol{A})(t-r)\tag{46}$$

$$\boldsymbol{\mu}(t)=(\boldsymbol{J}_L\otimes\boldsymbol{K})\boldsymbol{\chi}(t-d_i+\rho_i r+r_i)+(\boldsymbol{J}_L\otimes\boldsymbol{K})\boldsymbol{\chi}(t-d_i+(\rho_i-1)r+r_i)\tag{47}$$

Next, according to (44), (45), and (46), we obtain the dynamics of the closed-loop NMG as:

$$\begin{cases}\begin{bmatrix}\boldsymbol{\Omega}_0 & -(\boldsymbol{I}_N\otimes\boldsymbol{B})z^{-h}\\\bar{\boldsymbol{\Phi}}_{21}(z) & \boldsymbol{\Omega}_1\end{bmatrix}\begin{bmatrix}\boldsymbol{X}(z)\\\boldsymbol{U}(z)\end{bmatrix}=\boldsymbol{0}\\\bar{\boldsymbol{\Phi}}_{21}(z)=(\boldsymbol{J}_L\otimes\boldsymbol{K}_r)F(\rho_i-1,z)+(\boldsymbol{J}_L\otimes\boldsymbol{K})\boldsymbol{F}(\rho_i,z)\\\bar{\boldsymbol{\Phi}}_{22}(z)=(\boldsymbol{J}_L\otimes\boldsymbol{K})H(\rho_i,z)+(\boldsymbol{J}_L\otimes\boldsymbol{K}_r)\boldsymbol{H}(\rho_i-1,z)\\\boldsymbol{\Omega}_0=\boldsymbol{I}_N\otimes(z\boldsymbol{I}_N-\boldsymbol{A})-(\boldsymbol{I}_N\otimes\boldsymbol{A}_r)z^{-r}\\\boldsymbol{\Omega}_1=-(\boldsymbol{I}_N\otimes\boldsymbol{I}_m)+\bar{\boldsymbol{\Phi}}_{22}(z)(\boldsymbol{I}_N\otimes\boldsymbol{B})\end{cases}\tag{48}$$

Based on [35], characteristics of (48) can be represented as:

$$\Delta(z)=\det\begin{bmatrix}\boldsymbol{\Omega}_0 & -(\boldsymbol{I}_N\otimes\boldsymbol{B})z^{-h}\\\bar{\boldsymbol{\Phi}}_{21}(z) & \boldsymbol{\Omega}_1\end{bmatrix}=0\tag{49}$$

Then, for the simplified function $\Delta(z)$, we have:

$$\begin{aligned}&\bar{\boldsymbol{\Phi}}_{21}(z)+z^h\bar{\boldsymbol{\Phi}}_{22}(z)\boldsymbol{\Omega}_0=z^h((\boldsymbol{J}_L\otimes\boldsymbol{K})\boldsymbol{H}(\rho_i,z)+\\&(\boldsymbol{J}_L\otimes\boldsymbol{K}_r)\boldsymbol{H}(\rho_i-1,z))\boldsymbol{\Omega}_0+(\boldsymbol{J}_L\otimes\boldsymbol{K}_r)\boldsymbol{F}(\rho_i-1,z)+\\&(\boldsymbol{J}_L\otimes\boldsymbol{K})\boldsymbol{F}(\rho_i,z)=(\boldsymbol{J}_L\otimes\boldsymbol{K})z^{-d_i+\rho_i r+r_i}+(\boldsymbol{J}_L\otimes\boldsymbol{K}_r)z^{-d_i+(\rho_i-1)r+r_i}\end{aligned}\tag{50}$$

Considering (48), we can obtain:

$$\begin{aligned}\Delta(z)=&\det\begin{bmatrix}\boldsymbol{I}_N\otimes\boldsymbol{I}_n & \boldsymbol{0}\\z^h\bar{\boldsymbol{\Phi}}_{22}(z) & \boldsymbol{I}_N\otimes\boldsymbol{I}_m\end{bmatrix}\cdot\det\begin{bmatrix}\boldsymbol{\Omega}_0 & -(\boldsymbol{I}_N\otimes\boldsymbol{B})z^{-h}\\\bar{\boldsymbol{\Phi}}_{21}(z) & \boldsymbol{\Omega}_1\end{bmatrix}=\\&(-1)^{Nm}\prod_{i=2}^{N}\left|z\boldsymbol{I}_N-(\boldsymbol{A}+\lambda_i\boldsymbol{B}\boldsymbol{K})-(\boldsymbol{A}_r+\lambda_i\boldsymbol{B}\boldsymbol{K}_r)z^{-r}\right|\end{aligned}\tag{51}$$

Note that we transform the stability analysis of the closed-loop NMG consisting of (17) and (36) into the system stability analysis presented in (22). Recalling Assumption 2, we

have $\lim_{t\to\infty}\boldsymbol{\chi}_i(t)=\mathbf{0}$ and $\boldsymbol{x}(t)=(\bar{\boldsymbol{\Phi}}\otimes\boldsymbol{I}_n)\boldsymbol{\chi}(t)$. Then, we define $\mathbf{1}_N$ as the first column of $\bar{\boldsymbol{\Phi}}$, which means that $\lim_{t\to\infty}\boldsymbol{x}_i(t)=\boldsymbol{\chi}_1(t)$, $i=1,2,...,N$. The proof is completed.

IV. Experimental Results

This section provides four case studies to validate the robustness and superiority of the proposed SFC strategy in resisting multiple types of time delays. The experimental test setup utilized in this paper is depicted in Fig. 4, which mainly consists of a hardware circuit, a dSPACE controller, and a host computer.

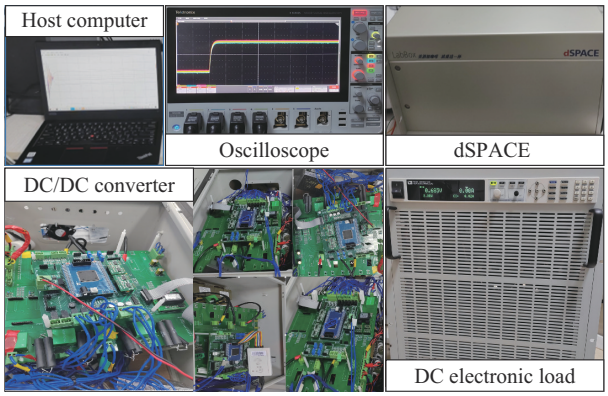

Fig. 4. Experimental test setup.

The hardware circuit consists of power supplies, DC/DC converters with LC filters, a DC electronic load, and transmission lines that connect the DREs. We construct the model of the test system in the MATLAB environment, and set multiple types of time delays through the delay module in the Simulink. Meanwhile, the MATLAB/Simulink model and the dSPACE real-time system are connected through real-time interface (RTI) in the dSPACE software environment, and then the automatic download of real-time hardware code from Simulink models to dSPACE can be achieved through the extended real-time workshop (RTW). The configuration of the NMG closely resembles that depicted in Fig. 1 and the parameters of the NMG are given in Table I.

A. Performance Verification

The numerical example provided in this subsection serves to validate the feasibility of the proposed SFC strategy. We consider four HESUs as individual agents, whose dynamics are represented by (1) and characterized by the following parameters.

$$\boldsymbol{A}=\begin{bmatrix}0.5 & 0.5 & 0 & 0\\ 0 & 0 & 0.5 & 0\\ 0 & 0 & 0.5 & 0\\ 0 & 0 & 0 & 1\end{bmatrix} \tag{52}$$

$$\boldsymbol{B}=[0 \quad 0.5 \quad 0 \quad 0.5]^{\mathrm{T}} \tag{53}$$

$$\boldsymbol{A}_r=\begin{bmatrix}-0.3041 & -2.845 & 3.152 & 0.2369\\ 0.2819 & 9.647 & -9.753 & -0.1722\\ 0.2716 & 9.412 & -9.506 & -0.1654\\ 0 & 0 & 0.0100 & 0.0200\end{bmatrix} \tag{54}$$

TABLE I
Parameters of NMG

Symbol	Value
V_{nom}	400 V
L_{line}	0.15 Ω
C_B	8.00 mF
L_B	1.00 mH
a_{ij}	5.00
k_{PV}	0.05
k_{IV}	95.00
k_{IP}	1.00
SOC_{H}	0.80
SOC_{L}	0.20
r_{HESU1}	0.10 Ω
r_{HESU2}	0.13 Ω
r_{HESU3}	0.15 Ω
r_{HESU4}	0.20 Ω

$$\boldsymbol{C}=[-1 \quad 0 \quad 0 \quad 1] \tag{55}$$

In this case, the communication delays are randomly given by $d_1=d_3=1$ and $d_2=d_4=2$. The state delay $r=2$ and the input delay $h=3$. The communication topology in this subsection is illustrated in Fig. 5, and the Laplacian matrix can be further obtained as:

$$\boldsymbol{L}=\begin{bmatrix}2 & 0 & -1 & -1\\ -1 & 1 & 0 & 0\\ -1 & -1 & 2 & 0\\ 0 & 0 & -1 & 1\end{bmatrix} \tag{56}$$

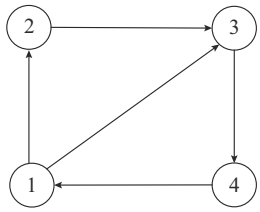

Fig. 5. Communication topology.

We further choose the eigenvalues of $\boldsymbol{L}$ as 0, 2, 2, and 2. Moreover, based on Lemma 2, we have the following state feedback gains:

$$\boldsymbol{K}=[-0.0121 \quad -0.0079 \quad -0.0009 \quad -0.0948] \tag{57}$$

$$\boldsymbol{K}_r=[0.0001 \quad -0.0742 \quad 0.0760 \quad -0.0028] \tag{58}$$

Next, it can be obtained that:

$$\boldsymbol{u}_i(s)=0 \quad i=1,2,3,4,\ s=-\tau_i,-\tau_i+1,...,0 \tag{59}$$

$$\boldsymbol{x}_1(s)=[1 \quad -1 \quad 2 \quad 1]^{\mathrm{T}} \tag{60}$$

$$\boldsymbol{x}_2(s)=[-2 \quad 3 \quad -3 \quad 2]^{\mathrm{T}} \tag{61}$$

$$\boldsymbol{x}_3(s)=[4 \quad -2 \quad 2 \quad 3]^{\mathrm{T}} \tag{62}$$

$$\boldsymbol{x}_4(s)=[2 \quad 3 \quad -3 \quad 2]^{\mathrm{T}} \tag{63}$$

The state feedback differences between HESU 1 and other HESUs are presented in Fig. 6.

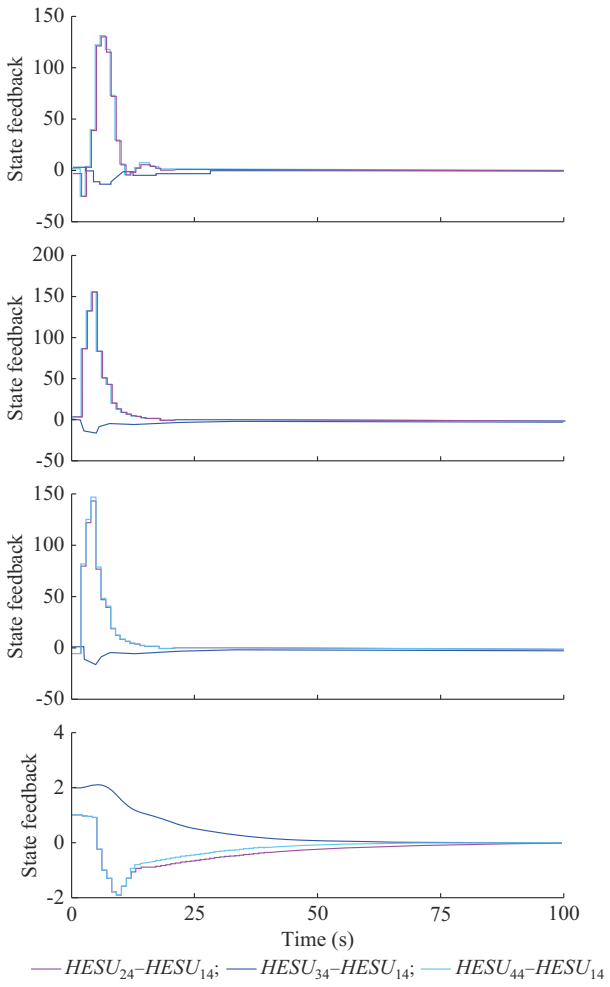

Fig. 6. State feedback differences between HESU 1 and other HESUs.

These results imply that the consensus of the HESUs can be achieved by implementing the proposed SFC strategy, which further demonstrates the correctness of Theorem 1. According to [15], it can be observed that all the voltages of the PCC buses converge to their nominal values if the communication network topology contains a directed spanning tree. Meanwhile, despite the presence of state delay, input delay, and communication delay in the NMG, the state convergence of HESUs can still be maintained. This implies that the proposed SFC strategy can effectively mitigate the influence of multiple types of time delays.

B. Control Performance with Different Light Intensities and Local Loads

In this subsection, we present experimental results to validate the control performance of the proposed SFC stragety. The time span for the case study is set between [0, 30]s. During the first stage, only the droop control is activated. At $t=9$ s, the proposed SFC strategy is implemented in the experimental case study of the NMG. Before $t=12$ s, the NMG is compelled to derive power from the HESUs owing to insufficient light intensity, the equilibrium between SOC and output power remains elusive at this moment. However, at $t=12$ s, the light intensity is enhanced by 750 W/m^2. It can be observed from Fig. 7 that the output power of the HESUs undergoes a significant reduction, yet it remains in a discharge state. Then, at $t=18$ s, the light intensity is further enhanced by 1800 W/m^2.

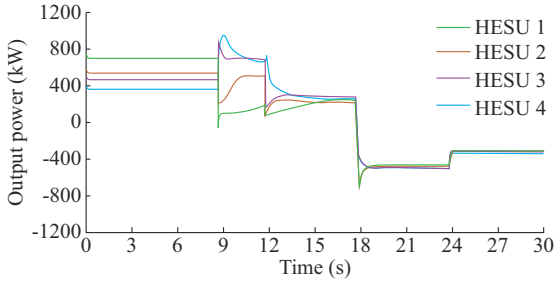

Fig. 7. Output power of HESU under different light intensities and local loads.

It can be observed from Fig. 7 that the NMG still has residual power after meeting the load demand. At this point, Fig. 8 indicates that the discharging state of the HESU is converted to the charging state. After a transient fluctuation process, the NMG can achieve SOC balance and accurate power allocation at the steady state. Furthermore, at $t=24$ s, we increase the local load by 450 kW. At this point, the light intensity is sufficient and the load power is being supplied by the PV system. The HESU does not have a direct role in power regulation, but the NMG can maintain SOC balance and ensure accurate power allocation.

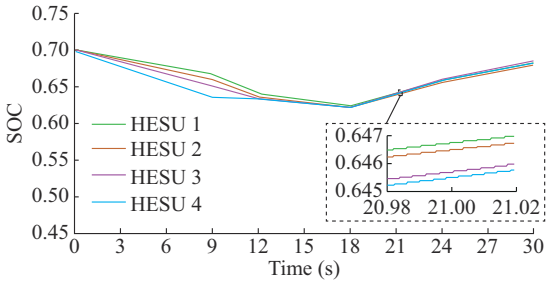

Fig. 8. SOC of HESU under different light intensities and local loads.

Figure 9 illustrates that the variations in light intensity result in significant fluctuations in the voltage of the PCC bus. However, the implementation of the proposed SFC strategy is capable of promptly regulating the voltage of the PCC bus to its nominal value. To summarize, the proposed SFC strategy can achieve accurate power allocation and meet the demand response of the NMG in real time under different light intensities and local loads.

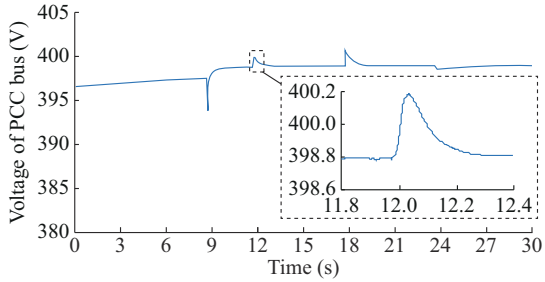

Fig. 9. Voltage of PCC bus of HESU under different light intensities and local loads.

C. Comparison with Multiple Types of Time Delays

To assess the robustness of the proposed SFC strategy, a comparison is made between dynamics based on the proposed DVC strategy and those based on the proposed SFC strategy with multiple types of time delays. Initially, the NMG operates stably under the primary control. Then, at $t=$ 10 s, we add multiple types of time delays to the NMG. In this case, the communication delay is chosen as 0.2 s. At this moment, the proposed SFC strategy comes into effect. The voltage of PCC bus and the change of Δv_i of the HESU with proposed DVC strategy are shown in Figs. 10 and 11, respectively. Δv_i further reflects the dynamic characteristics of the designed controller of the NMG.

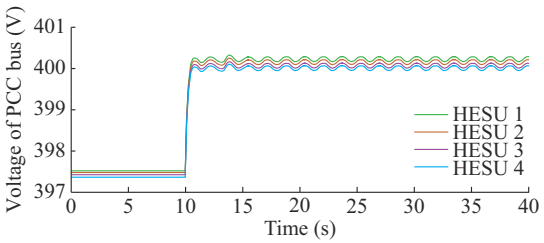

Fig. 10. Voltage of PCC bus of HESU with proposed DVC strategy.

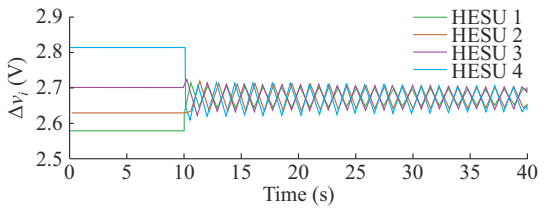

Fig. 11. Δv_i of HESU with proposed DVC strategy.

Moreover, under the influence of multiple types of time delays, the experimental results show that the NMG with proposed DVC strategy starts to oscillate without damping and becomes unstable. However, the HESUs of the NMG can still converge according to the proposed SFC strategy. The voltage of PCC bus and the change of Δv_i of the HESU with proposed SFC strategy are shown in Figs. 12 and 13, respectively.

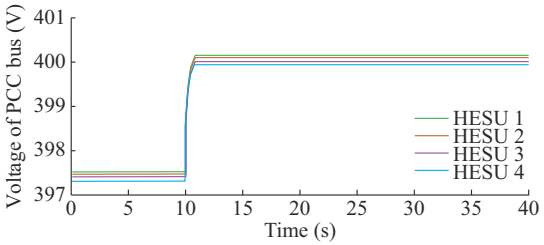

Fig. 12. Voltage of PCC bus of HESU with proposed SFC strategy.

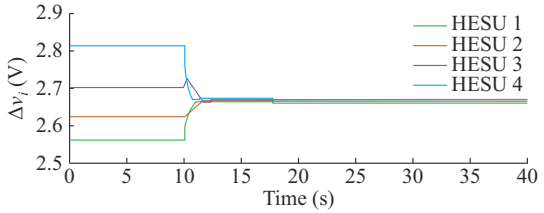

Fig. 13. Δv_i of HESU with proposed SFC strategy.

The NMG can maintain stable operation despite the presence of multiple types of time delays, albeit with a relatively slow convergence rate. We can observe from Fig. 10 that the voltage of the PCC bus of HESUs deviates from its nominal value with the proposed DVC strategy, which indicates that multiple types of time delays result in steady-state error in the NMG. Besides, the voltage of the PCC bus of HESUs with the proposed SFC strategy is shown in Fig. 12. It can be observed that the proposed SFC strategy can enable the voltage of PCC bus to recover to its nominal value, which indicates that the designed controller has no steady-state error. Meanwhile, the HESUs can converge to the steady-state value although there are multiple types of time delays. The above results validate that the proposed SFC strategy can effectively resist the impact of multiple types of time delays in the NMG. Therefore, compared with the proposed DVC strategy, the proposed SFC strategy exhibits superior robustness.

D. Comparison with Existing Control Methods

This subsection aims to demonstrate the superiority of the proposed SFC strategy. A case study of the NMG under step load is introduced to compare the proposed SFC strategy with the existing control methods. Specifically, the PV unit operates in the MPPT operation mode, and at $t=10$ s, four local loads with a resistance of 20 Ω are connected to the PCC bus. Figures 14 and 15 illustrate the control performance of the existing control method, while Figs. 16 and 17 demonstrate the control performance of the proposed SFC strategy. Figures 14 and 16 demonstrate that the HESUs of the NMG effectively stabilize the voltage fluctuations of the PCC bus caused by load fluctuations in a very short time. Comparatively, the proposed SFC strategy exhibits less voltage fluctuation of the PCC bus under load fluctuations compared with the existing control method. Moreover, Figs. 15 and 17 demonstrate that both the existing control method and the proposed SFC strategy can achieve power sharing. However, the proposed SFC strategy demonstrates a faster response speed under step load conditions compared with the existing control method. Based on these results, it can be concluded that the proposed SFC strategy exhibits rapid dynamic characteristics and high precision.

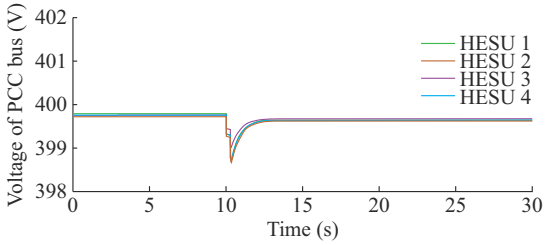

Fig. 14. Voltage of PCC bus of HESU with existing control method.

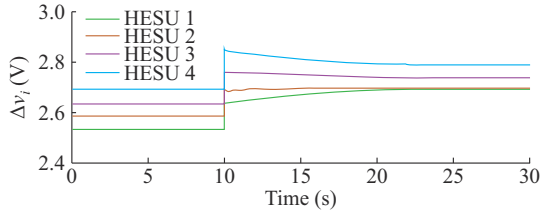

Fig. 15. Δv_i of HESU with existing control method.

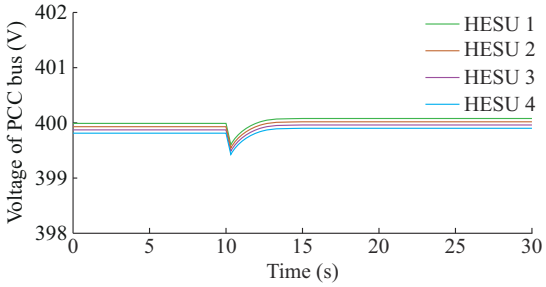

Fig. 16. Voltage of PCC bus of HESU with proposed SFC strategy.

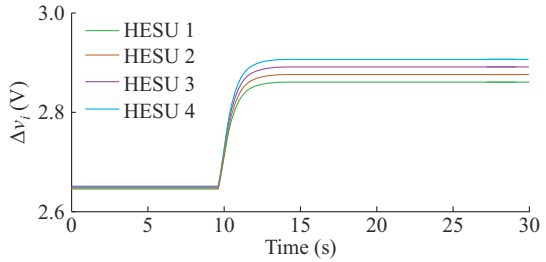

Fig. 17. Δv_i of HESU with proposed SFC strategy.

The performance of different methods in the NMG is then analyzed with multiple types of time delays. Initially, the NMG operates stably under the primary control. Then, at $t=10$ s, multiple types of time delays are added to the NMG, the communication delay is chosen as 0.3 s with the state delay $r=1$ s and the input delay $h=3$ s. At this moment, different control methods come into effect. When the control method in [14] is used, the NMG becomes unstable and exhibits divergent oscillations, as depicted in Figs. 18 and 19. Conversely, when implementing the proposed SFC strategy, the NMG still achieves consensus at a slower rate, as depicted in Figs. 20 and 21. These results verify that the proposed SFC strategy can effectively mitigate the influence of multiple types of time delays in the NMG.

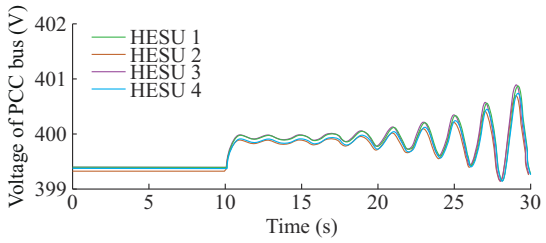

Fig. 18. Voltage of PCC bus of HESU with control method in [14].

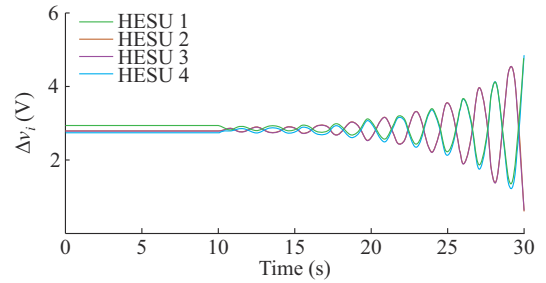

Fig. 19. Δv_i of HESU with control method in [14].

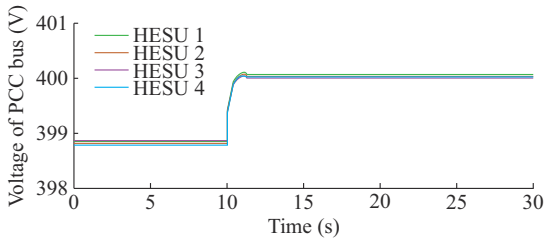

Fig. 20. Voltage of PCC bus of HESU with proposed SFC strategy.

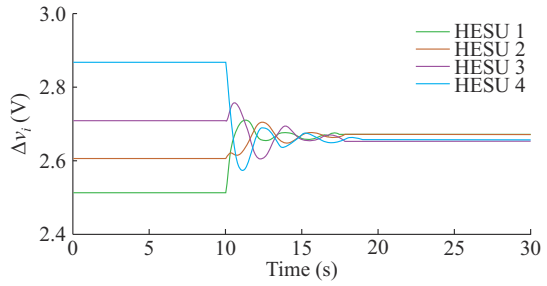

Fig. 21. Δv_i of HESU with proposed SFC strategy.

V. Conclusion

In this paper, an SFC strategy based on nested predictor is proposed to mitigate the influence of multiple types of time delays in the NMG. The proposed SFC strategy can distribute power according to the SOC of the HESUs while adjusting the average voltage of the PCC bus to its nominal value. In contrast to the proposed DVC strategy, the proposed SFC strategy can actively compensate for state, input, and communication delay. The experimental results demonstrate that the proposed SFC strategy can effectively mitigate the impact of time delays on system performance and enhance the stability of the NMG. In the future, we will further study and explore distributed control methods considering more complex NMGs.

References

[1] Q. Zhou, M. Shahidehpour, A. Alabdulwahab *et al*., "Flexible division and unification control strategies for resilience enhancement in networked microgrids," *IEEE Transactions on Power Systems*, vol. 35, no. 1, pp. 474-486, Jan. 2020.

[2] M. N. Ambia, K. Meng, W. Xiao *et al*., "Nested formation approach for networked microgrid self-healing in islanded mode," *IEEE Transactions on Power Delivery*, vol. 36, no. 1, pp. 452-464, Feb. 2021.

[3] Z. Li, M. Shahidehpour, F. Aminifar *et al*., "Networked microgrids for enhancing the power system resilience," *Proceedings of the IEEE*, vol. 105, no. 7, pp. 1289-1310, Jul. 2017.

[4] Y. Yu, G. Liu, and W. Hu, "Blockchain protocol-based secondary predictive secure control for voltage restoration and current sharing of DC microgrids," *IEEE Transactions on Smart Grid*, vol. 14, no. 3, pp. 1763-1776, May 2023.

[5] C. Deng, Y. Wang, C. Wen *et al*., "Distributed resilient control for energy storage systems in cyber-physical microgrids," *IEEE Transactions on Industrial Informatics*, vol. 17, no. 2, pp. 1331-1341, Feb. 2021.

[6] X. Li, G. Geng, Q. Jiang *et al*., "Consensus-based multi-converter power allocation strategy in battery energy storage system," *Journal of Energy Storage*, vol. 60, p. 106623, Apr. 2023.

[7] Z. Liu, B. Huang, X. Hu *et al*. (2023, Feb.) Blockchain-based renewable energy trading using information entropy theory. [Online]. Available: https://ieeexplore.ieee.org/abstract/document/10035496

[8] R. Wang, W. Li, Q. Sun *et al*., "Fully distributed dynamic edge-event-triggered current sharing control strategy for multibus DC microgrids

with power coupling," *IEEE Transactions on Industrial Informatics*, vol. 19, no. 4, pp. 5667-5678, Apr. 2023.
[9] X. Li, L. Lyu, G. Geng *et al*., "Power allocation strategy for battery energy storage system based on cluster switching," *IEEE Transactions on Industrial Electronics*, vol. 69, no. 4, pp. 3700-3710, Apr. 2022.
[10] K. Lai, Y. Wang, D. Shi *et al*., "Sizing battery storage for islanded microgrid systems to enhance robustness against attacks on energy sources," *Journal of Modern Power Systems and Clean Energy*, vol. 7, no. 5, pp. 1177-1188, Sept. 2019.
[11] F. Gao, R. Kang, J. Cao *et al*., "Primary and secondary control in DC microgrids: a review," *Journal of Modern Power Systems and Clean Energy*, vol. 7, no. 2, pp. 227-242, Mar. 2019.
[12] J. Zhou, M. Shi, X. Chen *et al*., "A cascaded distributed control framework in DC microgrids," *IEEE Transactions on Smart Grid*, vol. 12, no. 1, pp. 205-214, Jan. 2021.
[13] B. Huang, S. Zheng, R. Wang *et al*., "Distributed optimal control of DC microgrid considering balance of charge state," *IEEE Transactions on Energy Conversion*, vol. 37, no. 3, pp. 2162-2174, Sept. 2022.
[14] J. Zhou, Y. Xu, H. Sun *et al*., "Distributed event-triggered H_∞ consensus based current sharing control of DC microgrids considering uncertainties," *IEEE Transactions on Industrial Informatics*, vol. 16, no. 12, pp. 7413-7425, Dec. 2020.
[15] T. Morstyn, B. Hredzak, and V. G. Agelidis, "Distributed cooperative control of microgrid storage," *IEEE Transactions on Power Systems*, vol. 30, no. 5, pp. 2780-2789, Sept. 2015.
[16] Y. Li, H. Zhang, X. Liang *et al*., "Event-triggered-based distributed cooperative energy management for multienergy systems," *IEEE Transactions on Industrial Informatics*, vol. 15, no. 4, pp. 2008-2022, Apr. 2019.
[17] B. Huang, Y. Li, F. Zhan *et al*., "A distributed robust economic dispatch strategy for integrated energy system considering cyber-attacks," *IEEE Transactions on Industrial Informatics*, vol. 18, no. 2, pp. 880-890, Feb. 2022.
[18] D. L. Nguyen and H. H. Lee, "Accurate power sharing and voltage restoration in DC microgrids with heterogeneous communication time delays," *IEEE Transactions on Power Electronics*, vol. 37, no. 9, pp. 11244-11257, Sept. 2022.
[19] M. Shi, X. Chen, J. Zhou *et al*., "Distributed optimal control of energy storages in a DC microgrid with communication delay," *IEEE Transactions on Smart Grid*, vol. 11, no. 3, pp. 2033-2042, May 2020.
[20] W. Yao, Y. Wang, Y. Xu *et al*., "Small-signal stability analysis and lead-lag compensation control for DC networked-microgrid under multiple time delays," *IEEE Transactions on Power Systems*, vol. 38, no. 1, pp. 921-933, Jan. 2023.
[21] Q. Yang, J. Zhou, X. Chen *et al*., "Distributed MPC-based secondary control for energy storage systems in a DC microgrid," *IEEE Transactions on Power Systems*, vol. 36, no. 6, pp. 5633-5644, Nov. 2021.
[22] Z. Lian, C. Deng, C. Wen *et al*., "Distributed event-triggered control for frequency restoration and active power allocation in microgrids with varying communication time delays," *IEEE Transactions on Industrial Electronics*, vol. 68, no. 9, pp. 8367-8378, Sept. 2021.
[23] B. Huang, L. Liu, H. Zhang *et al*., "Distributed optimal economic dispatch for microgrids considering communication delays," *IEEE Transactions on Systems, Man, and Cybernetics: Systems*, vol. 49, no. 8, pp. 1634-1642, Aug. 2019.
[24] K. Li, C. Hua, X. You *et al*., "Output feedback-based consensus control for nonlinear time delay multiagent systems," *Automatica*, vol. 111, p. 108669, Jan. 2020.
[25] J. Peng, B. Fan, H. Xu *et al*., "Discrete-time self-triggered control of DC microgrids with data dropouts and communication delays," *IEEE Transactions on Smart Grid*, vol. 11, no. 6, pp. 4626-4636, Nov. 2020.
[26] E. A. Coelho, D. Wu, J. M. Guerrero *et al*., "Small-signal analysis of the microgrid secondary control considering a communication time delay," *IEEE Transactions on Industrial Electronics*, vol. 63, no. 10, pp. 6257-6269, Oct. 2016.
[27] H. J. Savino, C. R. P. dos Santos, F. O. Souza *et al*., "Conditions for consensus of multi-agent systems with time-delays and uncertain switching topology," *IEEE Transactions on Industrial Electronics*, vol. 63, no. 2, pp. 1258-1267, Feb. 2016.
[28] K. Li, C. Hua, X. You *et al*., "Distributed output-feedback consensus control for nonlinear multiagent systems subject to unknown input delays," *IEEE Transactions on Cybernetics*, vol. 52, no. 2, pp. 1292-1301, Feb. 2022.
[29] H. Zhang, H. Ren, Y. Mu *et al*., "Optimal consensus control design for multiagent systems with multiple time delay using adaptive dynamic programming," *IEEE Transactions on Cybernetics*, vol. 52, no. 12, pp. 12832-12842, Dec. 2022.
[30] Q. Liu and B. Zhou, "Consensus of discrete-time multiagent systems with state, input, and communication delays," *IEEE Transactions on Systems, Man, and Cybernetics: Systems*, vol. 50, no. 11, pp. 4425-4437, Nov. 2020.
[31] H. Chu, D. Yue, C. Dou *et al*., "Consensus of multiagent systems with time-varying input delay via truncated predictor feedback," *IEEE Transactions on Systems, Man, and Cybernetics: Systems*, vol. 51, no. 10, pp. 6062-6073, Oct. 2021.
[32] X. Yang and B. Zhou, "Consensus of discrete-time multiagent systems with input delays by truncated pseudo-predictor feedback," *IEEE Transactions on Cybernetics*, vol. 49, no. 2, pp. 505-516, Feb. 2019.
[33] Q. Liu and B. Zhou, "Delay compensation of discrete-time linear systems by nested prediction," *IET Control Theory & Applications*, vol. 10, no. 15, pp. 1824-1834, Oct. 2016.
[34] C. Dong, H. Jia, Q. Xu *et al*., "Time-delay stability analysis for hybrid energy storage system with hierarchical control in DC microgrids," *IEEE Transactions on Smart Grid*, vol. 9, no. 6, pp. 6633-6645, Nov. 2018.
[35] J. K. Hale, *Theory of Functional Differential Equations*. New York: Springer, 1977.
[36] W. Ren and Y. Cao, *Distributed Coordination of Multi-agent Networks, Communications and Control Engineering Series*. London: Springer, 2011.
[37] V. Nasirian, A. Davoudi, F. L. Lewis *et al*., "Distributed adaptive droop control for DC distribution systems," *IEEE Transactions on Energy Conversion*, vol. 29, no. 4, pp. 944-956, Dec. 2014.
[38] Z. Wang, F. Liu, Y. Chen *et al*., "Unified distributed control of standalone DC microgrids," *IEEE Transactions on Smart Grid*, vol. 10, no. 1, pp. 1013-1024, Jan. 2019.
[39] H. Luo and Z. Hu, "Stability analysis of sampled-data load frequency control systems with multiple delays," *IEEE Transactions on Control Systems Technology*, vol. 30, no. 1, pp. 434-442, Jan. 2022.
[40] L. Xu, Q. Guo, Z. Wang *et al*., "Modeling of time-delayed distributed cyber-physical power systems for small-signal stability analysis," *IEEE Transactions on Smart Grid*, vol. 12, no. 4, pp. 3425-3437, Jul. 2021.

Guoxiu Jing received the B.S. degree in electrical engineering and automation and the M.S. degree in control engineering from Nanchang University, Nanchang, China, in 2009 and 2013, respectively. She is currently pursuing the Ph.D. degree in School of Information Science and Engineering, Northeastern University, Shenyang, China. Her main research interests include energy storage, distributed cooperative control of microgrid system, and cyber-physical system.

Bonan Huang received the B.S. degree in electronic information engineering from Tianjin University, Tianjin, China, in 2005, and the M.Sc. and Ph.D. degrees in control theory and control engineering from Northeastern University, Shenyang, China, in 2008 and 2014, respectively. He is currently an Associate Professor with the School of Information Science and Engineering, Northeastern University. His main research interests include collaborative control and operation optimization of Energy Internet, multi-energy system, and cyber-physical security analysis of smart energy system.

Rui Wang received the B.S. degree in electrical engineering and automation and the Ph.D. degree in power electronics and power drive from Northeastern University, Shenyang, China, in 2016 and 2021, respectively. He is currently an Associate Professor with the School of Information Science and Engineering, Northeastern University. His main research interests include collaborative optimization of distributed generation and its stability analysis of electromagnetic timescale in cyber-energy system.

Chao Yang received the Ph.D. degree in computer applications technology from Dalian Maritime University, Dalian, China, in 2016. He is currently an Engineer with the Information and Communication Branch, State Grid Liaoning Electric Power Company Ltd., Shenyang, China. His main research interests include smart grid informatization, Internet-of-Things, and artificial intelligence.

Qiuye Sun received the Ph.D. degree in control theory and control engineering from Northeastern University, Shenyang, China, in 2007, where he has been a Full Professor and the Ph.D. Supervisor since 2014. His current research interests mainly include modeling and optimal operation of Energy Internet, complementary optimization of multi-energy system, and network control of distributed generation system.